Journal of Non-Crystalline Solids 447 (2016) 1–8

Contents lists available at ScienceDirect

Journal of Non-Crystalline Solids

journal homepage: www.elsevier.com/locate/jnoncrysol

Molecular dynamics simulations of amorphous silica surface properties with truncated Coulomb interactions

William Gonçalves [a,b,*], Julien Morthomas [a], Patrice Chantrenne [a], Michel Perez [a], Geneviève Foray [a], Christophe L. Martin [b]

[a] Université de Lyon, INSA-Lyon, CNRS, MATEIS, 7, Avenue Jean Capelle, 69621 Villeurbanne cedex, France
[b] Univ. Grenoble Alpes, CNRS, SIMAP, F-38000 Grenoble, France

ARTICLE INFO

Article history:
Received 8 January 2016
Received in revised form 14 April 2016
Accepted 9 May 2016
Available online 19 May 2016

Keywords:
Molecular dynamics
Amorphous silica
Surface energy
Aerogel
BKS
Cluster

ABSTRACT

Molecular Dynamics simulations have been performed to evaluate the capacity of the van Beest, Kramer and van Santen (BKS) [1] potential with truncated Coulomb interactions as proposed by A. Carré et al. [2] to reproduce amorphous silica surface properties. We compare the results obtained with the truncated BKS potential with those obtained from its full-range interaction version. Energies of $(SiO_2)_n$ clusters are computed for both potentials. The energies and structural properties of small aggregates of silica (from ≈3.5 nm to 7.6 nm of diameter) are investigated at high temperature. Both potentials lead to the same results for those properties when considering the transition from the core to the shell of aggregates. The significant computation time saved with this cut-off on Coulomb interactions allows for large-scale simulations of silica aerogels.

1. Introduction

Silica aerogels are highly nanoporous materials structured into a tortuous three-dimensional silica network. This high porosity can reach up to 99% with hypercritical drying [3]. Typically, 80% of the nano-size of pores is <30 nm which is at the origin of their very low thermal conductivity [4]. These super-insulation properties come at the price of poor mechanical properties. Nevertheless, these materials are used in various applications such as heat barriers, insulation panels for buildings, microelectronics, optics and acoustic devices [5,6]. Many experimental [7–10] and modeling [11–14] studies cover various aspects of the mechanical behavior of this important class of materials. However there is still a lack of sound knowledge on the mechanical properties due to the multiscale nature of the porosity network and of the particles.

Molecular Dynamics (MD) is an atomistic simulation method well suited to study mechanical properties at nano-scale. However, the full investigation of a system is limited by the size (volume of material) and by the duration (CPU time) of simulations. It is even more valid for materials with ionic interactions such as silica. These materials need Coulombic interactions to be computed for long-range distances at a great cost in terms of computation time. Focusing on highly porous silica aerogels, most studies dealt with volumes of material smaller than 20^3 nm^3 [12,15,16,17]. Such small volumes are hardly representative of the whole structure. Campbell et al. [11] attempted a large-scale simulation (36^3 nm^3) with a density of 1670 kg·m^{-3} (25% porosity) but it still leads to a low surface area compared to real aerogels. A recent study [18] dealing with thermal properties of silica aerogel exemplifies the constraints on MD simulations to reach realistic microstructures. Although the authors were able to reproduce successfully the power-law variation of thermal conductivity with density, they could not simulate samples with sufficiently large pores to compare directly with experimental observations. This is because several millions of atoms and systems with a length scale of hundred nanometers would have been required whereas <60.000 atoms were used in their study. Clearly, further progress in the simulation of silica areogels properties requires reliable potentials that allow for much larger MD simulations.

Concerning mechanical properties, a solution adopted by Ferreiro and Gelb [13,19] to get around the scaling problem consists in using Coarse-Grained Molecular Dynamics. Their model allows for the investigation of larger systems created with primary particles that interact through weak nonbonded forces and strong interparticle bonds. However the contact laws between primary particles during a simulated mechanical test need to be more realistic and accurate. Atomistic simulations that describe all interactions between atoms could advantageously be used as input for such Coarse-Grained simulations. In this context, the aim of our study is to demonstrate that using an effective interatomic potential in MD simulations, it is possible to simulate reasonably large volumes of material with high surface area.

* Corresponding author at: Université de Lyon, INSA-Lyon, CNRS, MATEIS, 7, Avenue Jean Capelle, 69621 Villeurbanne cedex, France.
E-mail address: william.goncalves@tutamail.com (W. Gonçalves).

http://dx.doi.org/10.1016/j.jnoncrysol.2016.05.024
0022-3093/

Various MD studies have focused on silica surfaces since the early eighties. Garofalini is one of the pioneer in this research area through his investigations on structure and diffusion of amorphous silica surface [20–23]. Garofalini has also investigated water adsorption with Mahadevan [24] and protonation of bridging oxygen sites with Lockwood [25]. In these two studies, a dissociative water potential with Wolf summation method has been used in order to truncate long-range Coulomb interactions. Ma et al. study [26] have discussed the convergence behavior of Wolf summation method. More recently, Rarivomanantsoa et al. [27] and Roder et al. [28] have investigated surface properties of thin silica film through MD simulations using the van Beest, Kramer and van Santen (BKS) potential [1]. The structures obtained with the BKS potential are close to those from *ab initio* calculations [29] that reveal the natural emergence of two-membered rings at the surface. Surface energies calculated by Roder et al. are also in good agreement with experimental values [30]. Mischler et al. [31] have compared in detail the structure of amorphous silica surfaces obtained with the BKS potential with *ab initio* molecular dynamics simulations using the Car-Parinello method (CPMD). They found a higher concentration of two-membered rings with the BKS potential as compared with the CPMD. For small scales (<5 Å), *ab initio* calculations are predictably more accurate for the simulation of the structure of silica surfaces. However, their results indicated that the structures obtained with both methods do not differ beyond 5 Å. When considering the need for an interatomic potential for silica [32] able to reproduce both bulk and surface properties of the amorphous phase at nano-scale, the BKS potential is a natural choice.

A recent study on silica bulk using BKS potential [33] showed that the contribution of long-range Coulomb interactions to the total energy is lower for the amorphous phase than for the crystalline phase at the same density. These recent results are in good agreement with the successful truncation of Coulomb interactions of BKS potential for amorphous phase [2]. This new potential truncated by Carré et al. [2] with Wolf shift method has been fitted on the original BKS potential to reproduce amorphous silica bulk properties. The benefits of this truncation compared to the computation of the full Ewald summation have already been discussed by Fennell et al. [34]. These authors have demonstrated that the results obtained with such a truncation method are in good agreement with those given by the full Ewald summation method for bulk systems. However, it is still an open question whether such a truncation is reliable for systems with free surfaces.

Here, we demonstrate that this new version of BKS without Coulomb long-range interactions [2] is able to reproduce the same silica surface properties as the original BKS potential. The significant saving in computation time could be used to study larger volumes of silica aerogels. All simulations have been performed with Large-scale Atomic/Molecular Massively Parallel Simulator (LAMMPS) [35].

2. Methods

2.1. Interatomic potentials

BKS is an empirical potential which includes a short-range contribution described by a Buckingham form and a long-range Coulombic contribution. It takes the general form for the interaction energy of atoms i and j:

$$\Phi_{BUCK}(r_{ij}) = a_{ij}\, exp(-b_{ij} r_{ij}) - \frac{c_{ij}}{r_{ij}^6},\ r_{ij} \le r_{cb} \tag{1}$$

$$\Phi_{BKS}(r_{ij}) = \frac{q_i q_j}{r_{ij}} + \Phi_{BUCK}(r_{ij}). \tag{2}$$

where q_i is the effective charge, r_{ij} the interatomic distance and a_{ij}, b_{ij}, and c_{ij} are short-range parameters [1]. The cut-off, r_{cb}, for short-range interactions is 5.5 Å. The BKS potential pertains to the Coulomb-Buckingham and thus does not tend to positive infinity when r tends to zero. At very high temperature, atoms may approach too close from each other which may induce chaotic dynamics. A solution consists in adding a 24–6 Lennard-Jones potential which is strongly repulsive at short distance [16,36] to prevent overlapping atoms.

$$\Phi_{LJ}(r_{ij}) = 4\varepsilon_{ij}\left[\left(\frac{\sigma_{ij}}{r_{ij}}\right)^{24} - \left(\frac{\sigma_{ij}}{r_{ij}}\right)^{6}\right],\ r_{ij} \le r_{cl} \tag{3}$$

where r_{cl} is the cut-off radius of 3 Å and ε_{ij}, σ_{ij} parameters which can be found in Ng's study [16]. Since there is no cut-off on Coulombic term, all contributions are computed. This study involves free surfaces and no periodic boundary conditions, thus, the Coulombic term is computed using the Multilevel Summation Method (MSM) [37]. Also, when using periodic boundary conditions, the evaluation of the Coulombic term by the Ewald summation method [38] is the most CPU-time consuming stage for large systems. The long-range contribution of this type of potential (BKS) can be advantageously truncated. Carré et al. [2] used the Wolf shift method to introduce a finite distance cut-off on Coulomb interactions. The Coulombic term in Eq. (2) is approximated by $\Phi_W(r_{ij})$:

$$\Phi_W(r_{ij}) = q_i q_j\left[\frac{1}{r_{ij}} - \frac{1}{r_{cw}} + \left(\frac{1}{r_{cw}^2}\right)(r - r_{cw})\right],\ r_{ij} \le r_{cw} \tag{4}$$

where r_{cw} is the cut-off on Coulomb interactions. The original Wolf shift is based on the screening of the charge contained in the cut-off sphere by placing an opposite charge on its surface. Eq. (4) is a modified version of Wolf shift method which has been proposed by Fennell et al. [34]. It ensures the continuity of both the potential and the forces at the cut-off radius, which was the main concern for the original Wolf shift. This Wolf shift method differs from the full Wolf summation used by Garofalini et al. [24,25] by applying a shift to the Coulomb interactions without damping electrostatic interactions. Fennell et al. [34] have shown very good agreement between this method and the full Ewald summation. Thus, Carré et al. [2] have applied this truncation on the BKS potential. Static and dynamic properties of bulk liquid silica such as the radial distribution functions, the bond angle distributions, the structure factor and the vibrational density of states have been fitted on silica bulk using periodic boundary conditions from the original BKS to its truncated version (denoted as Wolf BKS). This study uses a revisited version of the Wolf BKS potential with smoothed interactions and short-range repulsion (to prevent atoms overlapping at high temperature). Moreover, repulsive interactions between Silicon atoms have also been added compared to the original BKS. Those model improvements are meant to correct some known defects of the original BKS and to smooth interactions near the cut-off radius. They do not change significantly the properties of silica bulk. The full analytical expression can be found in Shcheblanov et al. [39].

2.2. Analysis of SiO_2 clusters using molecular statics

Molecular Statics is used to compute energies of small clusters (monomers, dimers, trimers and tetramers). Surface effects play an increasing role as the size of the system decreases. Thus, it is of interest to reproduce small silica clusters and investigate their total and binding energies to other MD results and to Density Functional Theory (DFT). In that case, atoms are initially located at coordinates given by Harkless et al. [40] and a potential energy minimization is performed using a conjugate gradient technique. The total and binding energies after minimization at 0 K are compared to energies from Harkless using the Tsuneyuki et al. (TTAM) empirical potential [41] which also computes Coulomb interactions.

A simple monomer (Fig. 1) with symmetric linear form $D_{\infty h}$ is first studied. It is composed by a silicon atom in between two oxygen

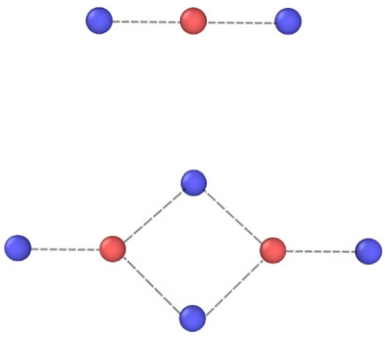

Fig. 1. Silica monomer with $D_{\infty h}$ symmetry (top) and dimer with D_{2h} symmetry (bottom). Silicon and Oxygen atoms are red and blue, respectively.

atoms. The second cluster is a dimer (Fig. 1), which is composed by two silicon atoms connected by a bridge of oxygen atoms. Two trimers with D_{3h} and D_{2d} symmetry are also investigated (Fig. 2). The first trimer exhibits a planar structure while the second trimer is a composition of two linked silica dimers in orthogonal planes.

Finally, two silica tetramers (Fig. 3) are studied. They may be considered as a composition of a trimer and a dimer. The first tetramer is a linear cluster with D_{2h} symmetry, and is a combination of D_{2d} trimer and a D_{2h} dimer. The second tetramer has a C_{2v} symmetry and is a combination of a D_{3h} trimer and a D_{2h} dimer. Both clusters are contained in two orthogonal planes. Larger and more complex silica clusters can be studied [40], however the aim here is not to investigate exotic clusters but to make sure that energies given by the two potentials are sound.

2.3. Investigation of silica aggregates properties using molecular dynamics

Molecular dynamics is used to study amorphous silica aggregates with a significant amount of free surface at high temperature. The simulation method is inspired from Roder's study [28] and results from BKS and Wolf BKS potentials are compared. Atoms of silicon and oxygen are initially randomly introduced inside a sphere, obeying silica stoichiometry and density ($\approx 2200\ \mathrm{kg\cdot m^{-3}}$). An energy minimization is performed in order to avoid overlapping of atoms and temperature is imposed to the system to complete the preparation stage. The integration of the equations of motion is achieved using a Verlet algorithm with a 1.6 fs timestep. Langevin thermostat [42] in the ensemble NVT is applied to control the dynamics of the system. In this study, the volume of the simulation box is much larger than the volume of the

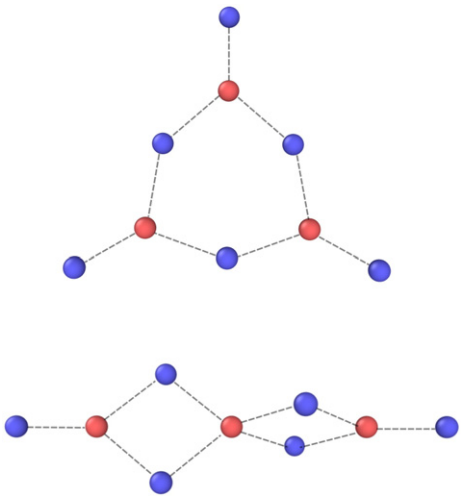

Fig. 2. Silica trimers with D_{3h} (top) and D_{2d} (bottom) symmetry.

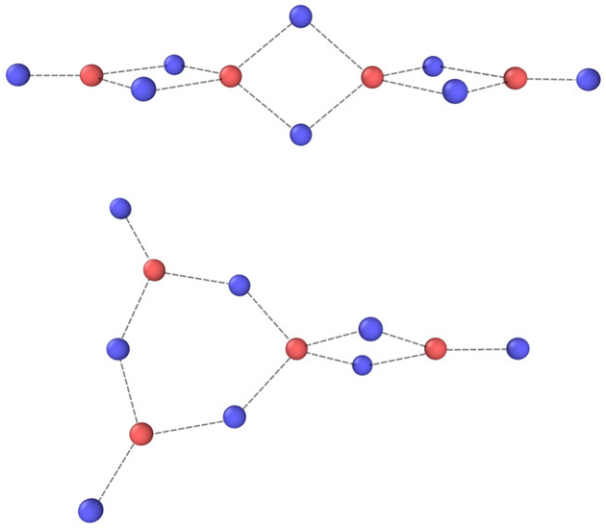

Fig. 3. Silica tetramers with D_{2h} (top) and C_{2v} (bottom) symmetry.

aggregate. This volume (and the density) can vary while the volume of the simulation box is conserved, due to the large amount of free surface. We increase the temperature of the structure from 0 K to a maximum temperature (T_{max}) in 40,000 timesteps. Keeping the temperature constant at T_{max}, the average potential energy is calculated over 60,000 timesteps (denoted as the relaxation phase). Note that the linear and angular momenta are set to zero every 100 timesteps to avoid rigid body motion of the whole aggregate. Simulations have been performed at $T_{max} = 4300$ K, 4000 K, 3400 K, 3000 K and 2750 K. Three structures with increasing sizes have been studied, $N = 1296$, 4608 and 13,824 where N is the total number of atoms.

Potential energies are calculated and compared to those obtained from the bulk using periodic boundary conditions. This bulk structure has been generated by placing randomly Silicon and oxygen atoms with the correct stoichiometry and density ($2200\ \mathrm{kg\cdot mm^{-3}}$) in a simulation box with periodic boundary conditions. A minimisation of potential energy using conjugate gradient technique has then been performed to separate overlapping atoms. Finally, temperature is given to the system and an averaged potential energy is computed over the relaxation phase following the same procedure as with aggregates. The bulk contains 8016 atoms and is equilibrated in the NPT ensemble with a Berendsen barostat [43] and temperature is controlled with Langevin thermostat [42]. Since the total number of atoms for the bulk and for the aggregates are different, total potential energies are normalized by the total number of atoms. The difference of potential energy, Δe_{pot}, between bulk, e_{pot}^{bulk}, and aggregates energies, $e_{pot}(N)$ which depends on N due to different sizes of aggregates, is the surface energy, E_s:

$$\Delta e_{pot} \equiv e_{pot}(N) - e_{pot}^{bulk} = \frac{E_s}{N}. \tag{5}$$

The surface energy per unit area ε may be calculated from the surface of the aggregate, S, and the density, ρ, in number of atoms:

$$\frac{E_s}{N} = \frac{\varepsilon\, S}{N} = \frac{\varepsilon\, 4\pi r_0^2}{N}, \tag{6}$$

$$\frac{E_s}{N} = \varepsilon\, 4\pi \left(\frac{3}{4\pi\rho}\right)^{2/3} N^{-1/3}. \tag{7}$$

where S is approximated by the surface of a sphere of radius r_0 which is averaged in the three directions (Ox), (Oy), (Oz) of the aggregate's radius during the relaxation phase. The surface calculation is approximated since at high temperatures, aggregates are rough and would have a

tendency to evaporate for long simulation times. Also, the shape of aggregates is not perfectly spherical (Fig. 4).

In order to compare our results with those of Roder et al. [28], aggregates are subdivided in three zones: shell (blue color), transition and core zone (purple color). The shell thickness is 5 Å. The transition zone between shell and core regions has a thickness of 3 Å. Atoms located inside the core zone exhibit properties that can be compared to those of the silica bulk. Structural properties are then investigated with radial and angular distribution functions and with ring analysis. We focus hereafter on the shell and on the core of the aggregate.

3. Cluster analysis

The results for the total potential energy of clusters are listed in Table 1 for the Wolf BKS and the original BKS potentials. The energies of the monomer are used to compute the binding energies for each cluster (Fig. 5). Binding energy is defined as the energy necessary for n SiO_2 molecules to form a $(SiO_2)_n$ cluster, as proposed by Harkless et al. [40].

3.1. Monomer

After minimization, the bond length computed for Si—O is 1.43 Å for both BKS potentials. Harkless et al. [40] calculated a 1.46 Å bond length with the TTAM potential. Nayak et al. [44] obtained a value of 1.53 Å with DFT calculations. Some care should be exercised concerning these values since there is no experimental published data for isolated SiO_2 monomer.

3.2. Dimer

According to Fig. 5, both BKS potentials lead to the same value of binding energy for the dimer cluster. Harkless [40] found a total energy of −94.8 eV and a binding energy of −5.3 eV for the TTAM potential. Nayak [44] obtained an energy of −3.7 eV with DFT calculations. Even if both BKS potentials overestimate this value (as the TTAM potential does too), these results may be deemed acceptable considering that these empirical potentials have been fitted in order to reproduce bulk silica properties. For simple dimer molecules with dominating surface effects, the Wolf BKS potential lead to the same binding energy as the original BKS, demonstrating that the two potentials are essentially equivalent in terms of stability.

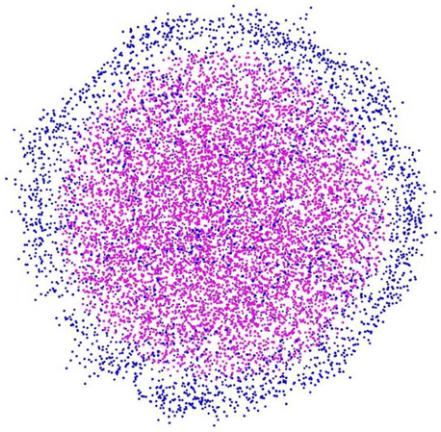

Fig. 4. View of an aggregate of amorphous silica. The shell zone is blue while the core is purple. Atoms from transition zone are not represented in this figure. $N = 13.824$, $T = 3000$ K.

Table 1
Total binding energies of $(SiO_2)_n$ clusters, which correspond to the total potential energy in Molecular Statics. Φ_{DMOL} stands for Nayak's DFT results [44] and Φ_{TTAM} for Harkless results [40] with TTAM potential.

[eV]	Φ_{DMOL}	Φ_{TTAM}	Φ_{BKS}	$\Phi_{Wolf\ BKS}$
Monomer ($D_{\infty h}$)	13.43	−44.7	−47.9	−36.2
Dimer (D_{2h})	30.56	−94.8	−102.5	−79.0
Trimer (D_{3h})	–	−145.6	−157.3	−122.0
Trimer (D_{2d})	48.12	−145.2	−157.4	−122.0
Tetramer (D_{2h})	65.65	−195.5	−212.2	−164.9
Tetramer (C_{2v})	–	−196.0	−212.2	−164.9

3.3. Trimers

Binding energies for silica trimers (Fig. 5) can be compared with those obtained by Raghavachari cited in Harkless's study using *ab initio* calculations [40]. Raghavachari's values are −8.2 eV and −9.2 eV for D_{3h} and D_{2d} clusters, respectively. As for the dimer, our results with BKS potentials are slightly larger than those obtained with the TTAM potential and *ab initio* calculations [40]. The same conclusion as for the resulting binding energies for dimer clusters can be drawn. Both trimers exhibit the same stability with BKS and Wolf BKS potentials.

3.4. Tetramers

The results for the binding energies of the tetramers are consistent with those for dimers and trimers. Both BKS potentials lead to the same energy to separate the cluster in n SiO_2 molecules which is still larger than the TTAM potential.

3.5. Discussion about cluster stability

The stability of all clusters is overestimated by BKS potentials, when comparing with the results of Harkless and Nayak. In order to compare with more accuracy these results with the DFT calculations of Nayak [44], we need to consider the total binding energy. We define it as the energy needed to separate the clusters into dissociated atoms. This total binding energy can be defined as:

$$E_b = E(SiO_2)_n - nE(Si) - 2nE(O) \quad (8)$$

where $E(..)$ are the total energies of clusters or atoms. Total energy of clusters in Molecular Statics corresponds to the total binding energy in Nayak's DFT results. As shown by Nayak [44], empirical interatomic potentials like TTAM [41] do not reproduce with accuracy energies of silica clusters while the structure and bond length are close to DFT results. In terms of total binding energies (Table 1), all empirical potentials exhibit

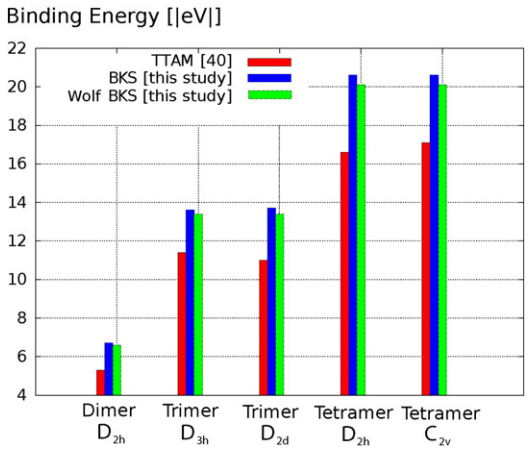

Fig. 5. Binding energies of clusters for various potentials.

overestimated values. However Wolf BKS is the closest to Nayak's DFT calculations [44]. The potential energy of Wolf BKS has been slightly shifted to lower values due to the truncation. This shift added to the positive (repulsive) interactions between Si—Si atoms in the Wolf BKS contribute to the lowering of absolute values of the total binding energies compared to original BKS.

In conclusion, this section demonstrates that the Wolf BKS is able to reproduce the same structure and energies of small SiO_2 clusters as the BKS potential. The energies necessary to form a $(SiO_2)_n$ cluster (Fig. 5) from n SiO_2 molecules are roughly comparable between all empirical potentials (mentioned in this study) and specially very close between both BKS potentials. Concerning total binding energies, they differ between all potentials. Since energies of Wolf BKS are closer to DFT results, the energetic description of this truncated potential for $(SiO_2)_n$ clusters may be considered more accurate than original BKS when considering the total binding energy.

4. Amorphous silica aggregates

Aggregates offer the possibility to test the ability of the Wolf BKS potential to describe the properties of amorphous silica surface. A natural application is then to generate nanoporous silica structure with high surface area and with a much larger volume. Ideally, since aerogels have a structure composed by a nanoporous solid skeleton, the potential should allow for the correct description of the structural properties both of the surface and of the bulk. Our reference for comparison of free surface properties is the original BKS [28]. Although this potential overestimates the number of rings $n = 2$ compared to *ab initio* calculations [31], the dynamics of free surfaces are well described in terms of energy and structural properties [31,28].

4.1. Energy characterization

The potential energies for the structures calculated with the Wolf BKS potential (normalized by N, the total number of atoms) for the three aggregates described in Section 2 are shown in Fig. 6, where solid lines are drawn as guides for the eyes. The difference between the bulk potential energy and the potential energy of aggregates, Δe_{pot}, increases with decreasing size of aggregates. This is because the contribution of the energy associated with the presence of a free surface increases with increasing surface to volume ratio. The inset in Fig. 6 plots $\frac{E_s}{N}$ *versus* $N^{-1/3}$ as calculated from Eq. (7). The lines in the inset are linear regressions of the data. Those results indicate that the slope decreases with increasing temperature. This is in accordance with experimental data [30] and with the results of Roder et al. [28].

Approximating the surface of the aggregate by a sphere of radius r_0, it is possible to compute the surface energy per unit aera ε. Using the original BKS potential for aggregates with $N = 1296, 4608, 13{,}824$, r_0 equals 16.8 Å, 26.1 Å and 38.2 Å, respectively. Values for the Wolf BKS potential are roughly the same with 17.5 Å, 26.2 Å and 37.9 Å. These are values of r_0 averaged over the relaxation phase and as discussed in Section 2, the shape of the aggregate is not perfectly spherical. These values of r_0 can be considered very close, keeping in mind the approximation of the surface. We have noticed that r_0 does not vary significantly with temperature. This is in accordance with the results of Roder et al. [28] who showed that this radius is weakly dependent on temperature since the thermal expansion coefficient of silica is small. For the bulk at 300 K, both BKS potentials exhibit the same density of 2200 $kg \cdot m^{-3}$ which is in good agreement with the experimental value of 2200 $kg \cdot m^{-3}$ at ambient temperature [30]. The density of these aggregates is 2000 $kg \cdot m^{-3}$, at the elevated temperatures investigated here, with both potentials. This means that the cut-off on long-range Coulomb interactions does not affect significantly the global density of aggregates for which free surface plays a substantial role.

The surface energy per unit area may be computed for each temperature from Eq. (7), using the density (in number of atoms N) and the slope of $\frac{E_s}{N}$ *versus* $N^{-1/3}$ (see inset of Fig. 6).

The experimental value for surface tension is 0.33 ± 0.04 $N \cdot m^{-1}$ at 2000 K [30]. Fig. 7 indicates that the surface energies calculated using either Wolf BKS or original BKS potential overestimate the experimental value, accounting for the difference in temperature. Indeed, we should keep in mind that ε can only provide an upper bound when considering entropic contribution to the free energy [28]. The slopes obtained in Fig. 7 are (-30.7 ± 5) $.10^{-3}$ $N \cdot m^{-1}$ per 100 K and (-10.7 ± 4) $.10^{-3}$ $N \cdot m^{-1}$ per 100 K for the BKS and for the Wolf BKS, respectively. The experimental value for the surface tension is -10.10^{-3} $N \cdot m^{-1}$ per 100 K [30]. Roder et al. [28] obtained a value of (-17 ± 9) $.10^{-3}$ $N \cdot m^{-1}$ per 100 K. Our results, obtained with original BKS potential, differ from those of Roder et al. First, it should be noted that there is a large uncertainty for the slope calculation. The results for the Wolf BKS underestimate the values of the original BKS potential. Although this comparison between both potentials is less satisfactory, the slope for Wolf BKS potential is closer to experimental value. Considering the computation time saved by using this truncated potential and the good agreement with the slope for experimentally derived surface energy, we believe that the Wolf BKS should be used instead of the original BKS potential when describing surface energy of amorphous silica.

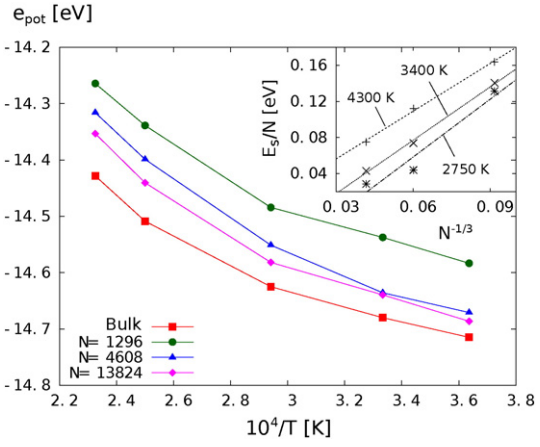

Fig. 6. Potential energy $e_{pot}[eV]$ *versus* $10^4/T[K]$ for Wolf BKS potential. The inset shows the dependence of surface energy $\Delta e_{pot} \equiv \frac{E_s}{N}$ with $N^{-1/3}$ according to Eq. (7) at 4300 K, 3400 K and 2750 K.

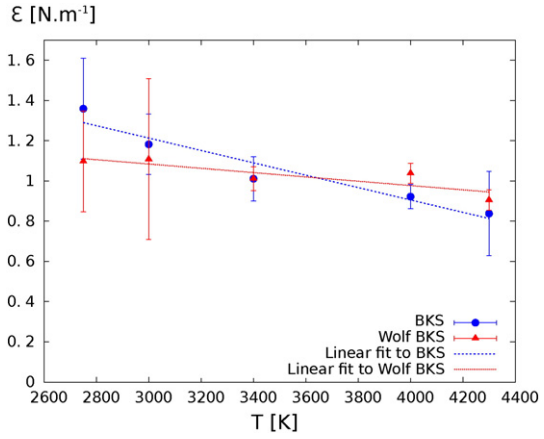

Fig. 7. Surface energy per unit area with both BKS potentials. Error bars are computed from the asymptotic standard error of linear regressions in the inset of Fig. 6.

4.2. Structural characterization

Structural properties are studied using the radial distribution function, the angular distribution function and rings distribution. In order to have statistically meaningful results, we compare these properties for the largest aggregate ($N = 13.824$) between the core and the shell. In accordance with the color code used in Fig. 4 for the illustration of the aggregate, a blue color is used for the shell zone and a purple one for the core zone for all subsequent graphs. Lines drawn on all graphs are guides for the eyes. Note that atoms of the transition zone between core and shell are not represented in Fig. 4. Structural properties have all been computed at 3000 K in order to compare with the results of Roder et al. [28].

Radial distribution functions (rdf) $g_{\alpha\beta}(r)$, which represents the probability of finding a pair of different atoms of type α,β separated by a distance r, are illustrated in Fig. 8. This function is normalized by $4\pi r^2$ in the silica bulk. For an heterogeneous system, this normalization [45] is adapted to ensure that $g_{\alpha\beta}(r)$ tends to unity when r goes to infinity. Moreover when α is picked in the shell, β can be chosen in a different zone (transition or core). This precaution is necessary since there are much fewer neighbors for long distances in the shell than in the core.

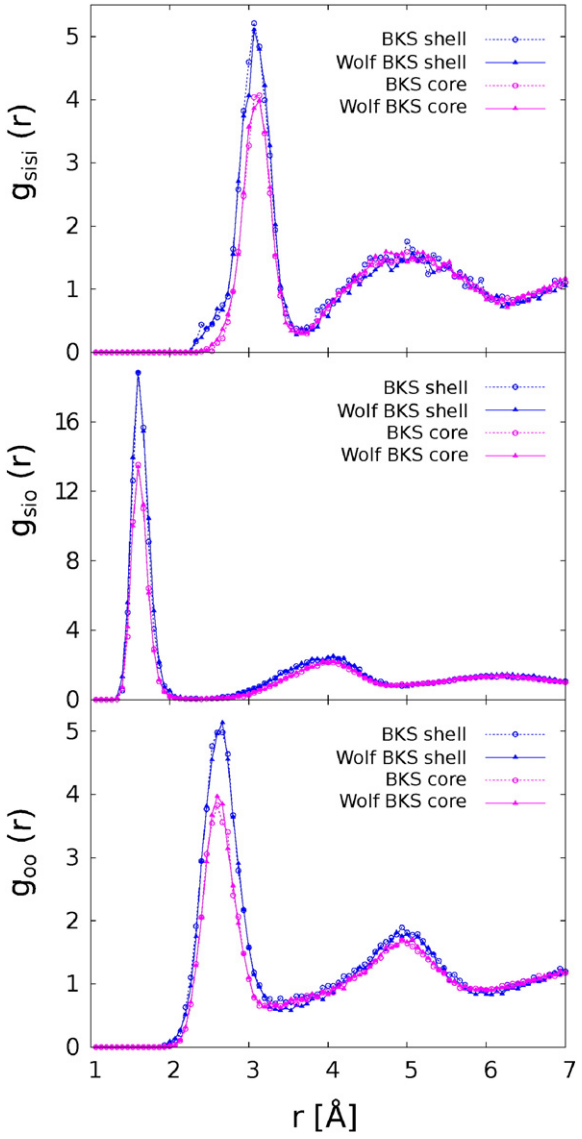

Fig. 8. Radial distribution functions $g_{\alpha\beta}(r)$ for both BKS potentials inside the aggregate (core) and on the surface (shell).

Both BKS potentials lead to more heterogeneous structures around the shell. This can be interpreted from the slightly broader first-neighbor peaks on the $g_{SiSi}(r)$ and $g_{OO}(r)$ functions. For $g_{SiO}(r)$, the distribution does not vary significantly from the bulk to the shell for both potentials. It means that those bounds are strong and do not depend on the surface environment. The $g_{SiSi}(r)$ at 2.5 Å exhibits a shoulder which only appears in the shell and which is consistent with Roder's and Rarivomanantsoa's results [28,27]. This shoulder is interpreted by these authors as the emergence of new rings $n = 2$ on the surface. It is interesting to note that those surface defects are reproduced by the Wolf BKS potential with accuracy compared to the BKS potential.

Angular distribution functions are plotted in Fig. 9. Angles compared in this study are intra-tetrahedral angles (OSiO) and inter-tetrahedral angles (SiOSi). For the first ones, the distribution can be assimilated to a gaussian function with a smaller standard deviation in the core than in the shell. This means that intra-tetrahedral angles are slightly more dispersive around 109 in the shell than in the core. The surface is then more heterogeneous due to surface effects. For inter-tetrahedral angles, we observe with both potentials a shift of approximately 10 towards smaller angles in the shell zone. Indeed these angles characterize the links between SiO_4 molecules. These links are easier to deform than those inside the SiO_4 tetrahedra. A new type of inter-tetrahedral angles at 100 is observed in the shell. Those new angles are related to the presence of rings $n = 2$ and to the shoulder previously mentioned in the $g_{SiSi}(r)$ rdf. Again, these results demonstrate that both BKS potentials exhibit the same behavior and lead to a more heterogeneous surface with the same characteristics.

The last structural property studied here is the rings size distribution. A ring is defined as the shortest closed path of consecutive Si—O elements. The first Si atom considered in the path is also the last one

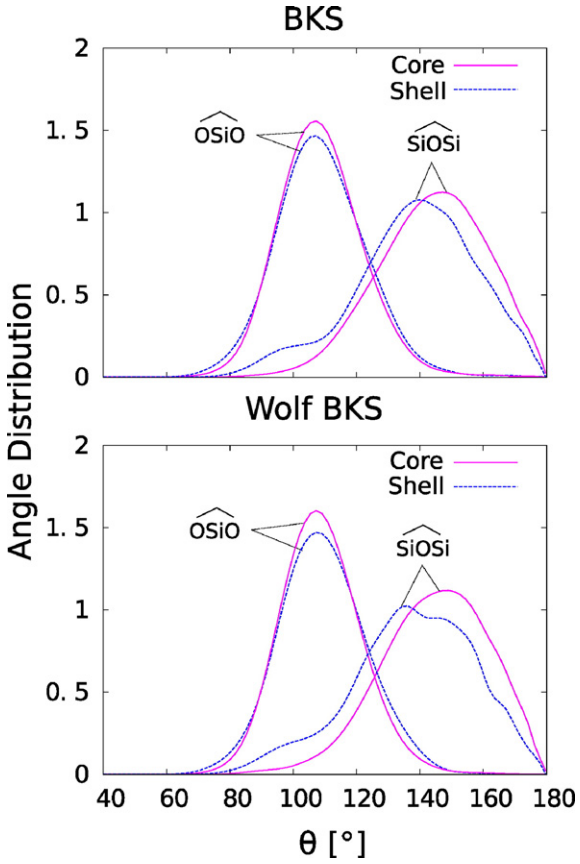

Fig. 9. Angular distribution functions, compared between core and shell of the aggregate with BKS and trunc. BKS potentials.

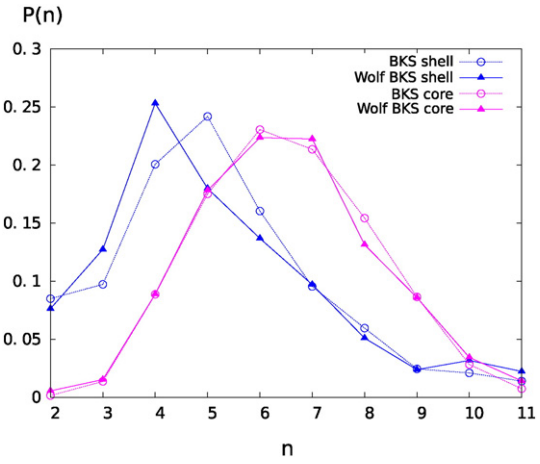

Fig. 10. Rings size distribution for the core and for the shell of the aggregate at 3000 K for both BKS potentials.

in order to obtain a closed ring. Only the primitive rings that cannot be decomposed into two smaller rings are considered to ensure the shortest closed path. Statistics on these rings have been computed with the R.I.N.G.S. code [46]. The size n of the ring is defined as the number of Si atoms in the closed path. Ring size distributions are plotted in Fig. 10 at 3000 K. They are similar to those obtained by Roder et al. [28]. In the core of the aggregate, in which structural properties are similar to those of a silica bulk, $n = 6$ leads to the highest probability for the BKS and Wolf BKS potentials. For smaller values of n, both BKS potentials give exactly the same values of $P(n)$. For larger n values, a slight dispersion can be observed. However the global trend remains similar. For the shell zone, the highest probability is given by $n = 5$ and $n = 4$ for the BKS and for the Wolf BKS, respectively. Fig. 10 indicates that the size of rings located around the shell is shifted towards smaller values for both potentials. This trend is more pronounced for Wolf BKS potential which exhibits higher values of $P(n)$ for $n = 3$ and $n = 4$. Since small rings are stiffer than large ones, we expect that the Wolf BKS potential leads to slightly stiffer macroscopic properties for the shell. Very small rings ($n = 2$ and 3), which were nearly absent of the bulk, are present in the shell for both potentials. This in accordance with the result of Roder et al. [28]. These short rings with small angles can be observed in the angular distribution functions (Fig. 9) and are linked to the apparition of the new inter-tetrahedral angles in the shell zone at 100. More generally, the evolution from the bulk to the shell of the ring size distributions is similar for both BKS potentials. We may expect that the shift towards smaller rings observed in the Wolf BKS potential will translate into slightly stiffer elastic properties for the shell, as compared to the initial BKS potential.

5. Wolf BKS potential for large volumes of silica aerogels

The experience gained on the utilization and on the properties of the widely used BKS potential should be beneficial for the investigation of the mechanical properties of silica aerogels. A recurring problem in molecular dynamics with these materials is the limited volume that can be simulated. Highly porous materials require sufficiently large volumes to allow for a correct assessment of their mechanical properties. Until now, the size of simulation boxes did not exceed 36 nm for mechanical studies [11]. Using the Wolf BKS potential, the enlargement of the simulation box is the focus of on-going simulations. Massively parallel simulations using box size of the order of 100 nm on an aerogel structure generated by negative pressure rupturing [47] are currently carried out (Fig. 11). This system contains >7.5 million of atoms with high surface area (90% of porosity), modelled with the validated bulk and surface properties of Wolf BKS potential.

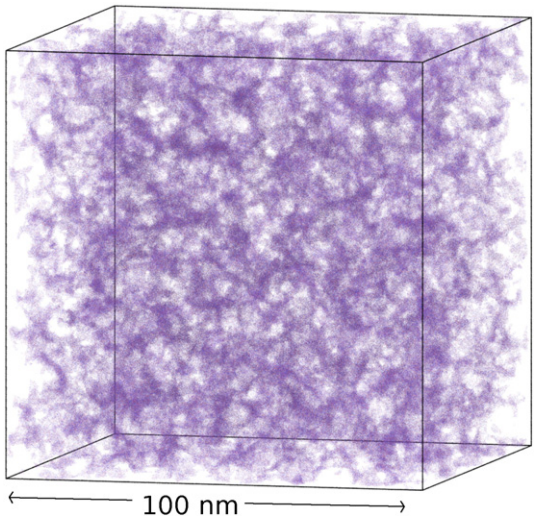

Fig. 11. Highly nanoporous structure (90% of porosity) with >7.5 million atoms generated using the Wolf BKS potential.

On the same CPU, a three orders of magnitude ratio in terms of CPU time per atom per step has been observed between BKS and Wolf BKS for the generation of aerogel structures with periodic boundary conditions. Typically 2 days are necessary to create this structure with 7.5 million of atoms (Fig. 11) on a parallel computer with Wolf BKS potential using 12 nodes, 192 processors. In the same conditions, the computation time needed to generate the same structure with original BKS would be more than a thousand days. These time and length scales reached by using the Wolf BKS potential open the possibility to investigate properly the mechanical properties of silica aerogel with atomistic simulations.

6. Concluding remarks

We have shown that the BKS potential with long-range Coulomb interactions truncated by Carré et al. [2] using Wolf's method can reproduce quite satisfactorily the same silica surfaces properties as the original BKS potential. The rationale for the choice of the widely used BKS potential is that previous studies have shown its ability to create amorphous silica surfaces with structural and energetic properties in good agreement with experimental data. Its truncated version allows for significant gain in computational time. More information on the benefits of Ewald truncation can be found in Fennell et al. [34] and Gdoutos et al. [48] studies. This provides an avenue for the simulation of larger volumes of material with high surface to volume ratio, and thus enables Molecular Dynamics studies of silica aerogel with several millions of atoms (Fig. 11), which to our best knowledge have not been attempted yet. In the future, such large simulations should allow direct comparison with 3D images of the nanostructure of silica aerogels [49].

In the extreme case of very high surface effects (small $(SiO_2)_n$ clusters), both BKS potentials lead to the same binding energies and results are comparable to those of Harkless et al. [40] obtained with the TTAM potential. However, it should be clear that these empirical potentials are not able to reproduce accurately the energies given by the more reliable DFT method for silica clusters. Indeed, we obtain noticeable differences with DFT for the total binding energies with both BKS potentials. Nevertheless, it is worth noting that the Wolf BKS potential results in energies that are closer to those of the DFT as compared to the original BKS. Also, isolated molecules were not generated in solid materials like silica aerogel.

Introducing temperature in our simulations allows for an assessment of the capability of these potentials to reproduce satisfactorily the energetic and structural properties of amorphous silica free surfaces. Simulations inspired from Roder et al. [28] have been carried out and

results, when considering energies, show less satisfactory comparison between both potentials. The description of the surface energy decrease with increasing temperature is in better agreement with experimental data when using the Wolf BKS potential than with the BKS potential. In terms of surface energy, there should be no restriction on using Wolf BKS potential instead of its original version.

Structural properties such as radial and angular distributions and ring analysis have been compared at 3000 K on the largest aggregate ($N = 4608$). The truncated version and the original BKS results in more heterogeneous and disordered structures in the shell, as it should. Ring distributions are shifted towards smaller rings when migrating from core to shell due to surface effects. In agreement with results from Roder et al., small rings ($n = 2.3$) appear in the shell with both potentials. The general behavior of the system, when considering the transition from the core to the shell of the aggregate, is very similar with both version of the BKS. Thus, our conclusion is that the cut-off on long-range interactions introduced by Carré [2] can be used without any significant loss of accuracy for systems with high surface effects.

Acknowledgments

Funding for this project was provided by a grant from la Région Rhône-Alpes (ARC Energies). We are thankful to FLMSN (Fédération Lyonnaise de Modélisation et Sciences Numériques). All simulations were performed on their massively parallel computer P2CHPD.

References

[1] B. Van Beest, G. Kramer, R. Van Santen, Force fields for silicas and aluminophosphates based on ab initio calculations, Phys. Rev. Lett. 64 (16) (1990) 1955.
[2] A. Carré, L. Berthier, J. Horbach, S. Ispas, W. Kob, Amorphous silica modeled with truncated and screened coulomb interactions: a molecular dynamics simulation study, J. Chem. Phys. 127 (11) (2007) 114512.
[3] T. Tillotson, L. Hrubesh, Transparent ultralow-density silica aerogels prepared by a two-step sol-gel process, J. Non-Cryst. Solids 145 (1992) 44–50.
[4] O.-J. Lee, K.-H. Lee, T.J. Yim, S.Y. Kim, K.-P. Yoo, Determination of mesopore size of aerogels from thermal conductivity measurements, J. Non-Cryst. Solids 298 (2–3) (2002) 287–292.
[5] Y. Akimov, Fields of application of aerogels (review), Instrum. Exp. Tech. 46 (3) (2003) 287–299.
[6] T. Burger, J. Fricke, Aerogels: production, modification and applications, Ber. Bunsenges. Phys. Chem. 102 (11) (1998) 1523–1528.
[7] M. Moner-Girona, A. Roig, E. Molins, E. Martnez, J. Esteve, Micromechanical properties of silica aerogels, Appl. Phys. Lett. 75 (5) (1999) 653–655.
[8] T. Woignier, J. Phalippou, Scaling law variation of the mechanical properties of silica aerogels, J. Phys. Colloq. 50 (C4) (1989) C4–179.
[9] A.H. Alaoui, T. Woignier, G.W. Scherer, J. Phalippou, Comparison between flexural and uniaxial compression tests to measure the elastic modulus of silica aerogel, J. Non-Cryst. Solids 354 (40) (2008) 4556–4561.
[10] M.-A. Einarsrud, E. Nilsen, A. Rigacci, G.M. Pajonk, S. Buathier, D. Valette, M. Durant, B. Chevalier, P. Nitz, F. Ehrburger-Dolle, Strengthening of silica gels and aerogels by washing and aging processes, J. Non-Cryst. Solids 285 (1) (2001) 1–7.
[11] T. Campbell, R.K. Kalia, A. Nakano, F. Shimojo, K. Tsuruta, P. Vashishta, S. Ogata, Structural correlations and mechanical behavior in nanophase silica glasses, Phys. Rev. Lett. 82 (20) (1999) 4018.
[12] J.S.R. Murillo, M.E. Bachlechner, F.A. Campo, E.J. Barbero, Structure and mechanical properties of silica aerogels and xerogels modeled by molecular dynamics simulation, J. Non-Cryst. Solids 356 (25) (2010) 1325–1331.
[13] C.A. Ferreiro-Rangel, L.D. Gelb, Computational study of uniaxial deformations in silica aerogel using a coarse-grained model, J. Phys. Chem. B 119 (27) (2015) 8640–8650.
[14] C.A. Angell, Forty years of silica simulations. Which way now? Int. J. Appl. Glas. Sci. 14 (2015) 3–14.
[15] J. Lei, Z. Liu, J. Yeo, T.Y. Ng, Determination of the Young's modulus of silica aerogels–an analytical–numerical approach, Soft Matter 9 (47) (2013) 11367–11373.
[16] T.Y. Ng, J.J. Yeo, Z. Liu, A molecular dynamics study of the thermal conductivity of nanoporous silica aerogel, obtained through negative pressure rupturing, J. Non-Cryst. Solids 358 (11) (2012) 1350–1355.
[17] S. Bhattacharya, J. Kieffer, Fractal dimensions of silica gels generated using reactive molecular dynamics simulations, J. Chem. Phys. 122 (9) (2005) 094715.
[18] J. Yeo, Z. Liu, T. Ng, Enhanced thermal characterization of silica aerogels through molecular dynamics simulation, Model. Simul. Mater. Sci. Eng. 21 (7) (2013) 075004.
[19] C.A. Ferreiro-Rangel, L.D. Gelb, Investigation of the bulk modulus of silica aerogel using molecular dynamics simulations of a coarse-grained model, J. Phys. Chem. B 117 (23) (2013) 7095–7105.
[20] S.H. Garofalini, Molecular dynamics computer simulations of silica surface structure and adsorption of water molecules, J. Non-Cryst. Solids 120 (1) (1990) 1–12.
[21] S. Garofalini, A molecular dynamics simulation of the vitreous silica surface, J. Chem. Phys. 78 (4) (1983) 2069–2072.
[22] D.A. Litton, S.H. Garofalini, Vitreous silica bulk and surface self-diffusion analysis by molecular dynamics, J. Non-Cryst. Solids 217 (2) (1997) 250–263.
[23] S. Levine, S.H. Garofalini, A structural analysis of the vitreous silica surface via a molecular dynamics computer simulation, J. Chem. Phys. 86 (5) (1987) 2997–3002.
[24] T. Mahadevan, S. Garofalini, Dissociative chemisorption of water onto silica surfaces and formation of hydronium ions, J. Phys. Chem. C 112 (5) (2008) 1507–1515.
[25] G.K. Lockwood, S.H. Garofalini, Bridging oxygen as a site for proton adsorption on the vitreous silica surface, J. Chem. Phys. 131 (7) (2009) 074703.
[26] Y. Ma, S. Garofalini, Modified wolf electrostatic summation: incorporating an empirical charge overlap, Mol. Simul. 31 (11) (2005) 739–748.
[27] M. Rarivomanantsoa, P. Jund, R. Jullien, Classical molecular dynamics simulations of amorphous silica surfaces, J. Phys. Condens. Matter 13 (31) (2001) 6707.
[28] A. Roder, W. Kob, K. Binder, Structure and dynamics of amorphous silica surfaces, J. Chem. Phys. 114 (17) (2001) 7602–7614.
[29] D. Ceresoli, M. Bernasconi, S. Iarlori, M. Parrinello, E. Tosatti, Two-membered silicon rings on the dehydroxylated surface of silica, Phys. Rev. Lett. 84 (17) (2000) 3887.
[30] O. Mazurin, M. Streltsina, T. Shvaiko-shvaikovskaya, Handbook of glass data silica glass and binary silicate glasses, part a 15, Part A 1983
[31] C. Mischler, W. Kob, K. Binder, Classical and ab-initio molecular dynamic simulation of an amorphous silica surface, Comput. Phys. Commun. 147 (1) (2002) 222–225.
[32] A.F. Combariza, D.A. Gomez, G. Sastre, Simulating the properties of small pore silica zeolites using interatomic potentials, Chem. Soc. Rev. 42 (1) (2013) 114–127.
[33] C. Rajappa, S.B. Sringeri, Y. Subramanian, J. Gopalakrishnan, A molecular dynamics study of ambient and high pressure phases of silica: structure and enthalpy variation with molar volume, J. Chem. Phys. 140 (24) (2014) 244512.
[34] C.J. Fennell, J.D. Gezelter, Is the ewald summation still necessary? Pairwise alternatives to the accepted standard for long-range electrostatics, J. Chem. Phys. 124 (23) (2006) 234104.
[35] S. Plimpton, Fast parallel algorithms for short-range molecular dynamics, J. Comput. Phys. 117 (1) (1995) 1–19.
[36] Y. Guissani, B. Guillot, A numerical investigation of the liquid–vapor coexistence curve of silica, J. Chem. Phys. 104 (19) (1996) 7633–7644.
[37] D.J. Hardy, J.E. Stone, K. Schulten, Multilevel summation of electrostatic potentials using graphics processing units, Parallel Comput. 35 (3) (2009) 164–177.
[38] P.P. Ewald, Die berechnung optischer und elektrostatischer gitterpotentiale, Ann. Phys. 369 (3) (1921) 253–287.
[39] N.S. Shcheblanov, B. Mantisi, P. Umari, A. Tanguy, Detailed analysis of plastic shear in the raman spectra of SiO_2 glass, J. Non-Cryst. Solids 428 (2015) 6–19.
[40] J.A. Harkless, D.K. Stillinger, F.H. Stillinger, Structures and energies of SiO_2 clusters, J. Phys. Chem. 100 (4) (1996) 1098–1103.
[41] S. Tsuneyuki, M. Tsukada, H. Aoki, Y. Matsui, First-principles interatomic potential of silica applied to molecular dynamics, Phys. Rev. Lett. 61 (7) (1988) 869–872.
[42] T. Schneider, E. Stoll, Molecular-dynamics study of a three-dimensional one-component model for distortive phase transitions, Phys. Rev. B 17 (3) (1978) 1302.
[43] H.J. Berendsen, J.P.M. Postma, W.F. van Gunsteren, A. DiNola, J. Haak, Molecular dynamics with coupling to an external bath, J. Chem. Phys. 81 (8) (1984) 3684–3690.
[44] S. Nayak, B. Rao, S. Khanna, P. Jena, Atomic and electronic structure of neutral and charged sinom clusters, J. Chem. Phys. 109 (4) (1998) 1245–1250.
[45] A. Roder, (Ph.d. thesis) (University of Mainz, 2000).
[46] S. Le Roux, P. Jund, Ring statistics analysis of topological networks: new approach and application to amorphous ges 2 and SIO 2 systems, Comput. Mater. Sci. 49 (1) (2010) 70–83.
[47] J. Kieffer, C.A. Angell, Generation of fractal structures by negative pressure rupturing of SIO 2 glass, J. Non-Cryst. Solids 106 (1) (1988) 336–342.
[48] E.E. Gdoutos, R. Agrawal, H.D. Espinosa, Comparison of the Ewald and Wolf methods for modeling electrostatic interactions in nanowires, Int. J. Numer. Methods Eng. 84 (13) (2010) 1541–1551.
[49] L. Roiban, G. Foray, Q. Rong, A. Perret, D. Ihiawakrim, K. Masenelli-Varlot, E. Maire, B. Yrieix, Advanced three dimensional characterization of silica-based ultraporous materials, RSC Adv. (December 2015) (Accepted in).